MAGNETOHYDRODINAMIC DUSTY HYBRID NANOFLUID PERISTALTIC FLOW IN CURVED CHANNELS

by

Sameh E. AHMED [a,b*] ***and Zenab Z. RASHED*** [c]

[a] Department of Mathematics, College of Science Abha,
King Khalid University, Abha, Saudi Arabia
[b] Department of Mathematics, Faculty of Science, South Valley University, Qena, Egypt
[c] Mathematics Department, Faculty of Science and Arts,
Jouf University, Qurayyat, Saudi Arabia

Original scientific paper
https://doi.org/10.2298/TSCI191014144A

This paper presents numerical simulations for a MHD convective process in curved channels. The worked suspension consists of water as a based hybrid nanofluid and two types of the nanoparticles, namely, Cu and Al_2O_3. Two systems of the governing equations are formulated for the hybrid nanofluid and dusty phases. The hybrid nanofluid system is modeled in view of lubrication approach. The governing equations are mapped to a regular computational domain then they solved numerically using the fourth order Runge-Kutta method. The obtained findings revealed that the growing in the Hartmann number causes a reduction in both of the hybrid nanofluid and dusty velocities while the mixture temperature is enhanced. Also, the temperature distributions are supported when either the Grashof number or the amplitude ratio is altered.

Key words: *MHD, peristaltic motion, dusty particles, hybrid nanofluid, curved channels*

Introduction

Various practical applications can be found for the peristalsis flow inside irregular domains. These applications include, for example, movement of the food in the intestine tract, the urine passage from a kidney to the bladder blood flow in small veins and arteries of the blood circulation, transferring the ovum in the Fallopian tube and the movement of sperm in the channels. Also, there are many applications of peristaltic motion in the biomedical devices, such as blood pumps and heart lung machines. In the related context, Latham [1], Mishra and Pandey [2] proposed the physiology of the gastrointestinal tract as an example for the peristalsis flow. Also, the peristaltic flows in curved channels were handled by several studies [3-11]. Sato *et al*. [3] discussed the peristaltic flow in a curved channel. Ali *et al*. [4] studied the peristaltic flow in a curved channel with a long wavelength approximation. Ali *et al*. [5, 6] examined effects of the heat transfer and fluid-flow of a non-Newtonian third grade fluid in a curved channel. Hayat *et al*. [7] discussed the Newtonian fluid peristaltic flow, heat and mass transfer in a curved channel with compliant walls. The investigation in [7] was extended by Hayat *et al*. [8] and Hina *et al*. [9] to include case of a third grade fluid. Hina *et al*. [9] considered case of the peristaltic motion in curved channels contain compliant walls using Johnson-Segalman fluid. Hina *et al*.

* Corresponding author, e-mail: sehassan@kku.edu.sa

[10, 11] examined the double diffusive together with impacts of the wall properties on the peristaltic flow of Johnson-Segalman and the peristaltic flow of pseudoplastic fluid, respectively.

Recently, the hybrid nanofluid which is considered as a novel type of the nanofluids received a major attention from the researchers due to their applications in various fields. The traditional nanofluid mixture is introduced for the first time by Choi [12] who studied the pure fluids with suspended nanoparticles. His results indicated to the substantial augmentation of the heat transported in suspensions of Cu or Al nanoparticles in water or other liquids. Additionally, the transport governing equations in which the Brownian motion and thermophores impacts were assumed have been presented by Buongiorno [13]. Using these types of mixtures, the peristaltic flows inside the curved channels are still few. Hina *et al*. [14] discussed numerically the peristaltic flow of a nanofluid in a curved channel. Ayub *et al*. [15] studied the mixed convection in the presence of a thermal radiation and a chemical reaction, analytically. The results indicated that the heat transfer rate decreases with the increase in thermophoresis parameter. Narla *et al.* [16] studied the peristaltic transport of a Jeffrey nanofluid in a curved channel and examined effects of various parameters on the fluid-flow and the temperature distributions. Noreen *et al*. [17] discussed the induced magnetic field effects on the peristaltic flow in a curved channel. They found that an increase in the Brownian motion and thermophoresis parameters causes an increase in the temperature profiles. Hayat *et al*. [18] studied the peristaltic motion of a Cu-water based nanoliquid with the thermal slip conditions. Hayat *et al.* [19] studied the MHD peristaltic flow of Sisko nanofluids with the Joule heating effects. They used a numerical treatment for the governing equations. They found that the increasing values of the curvature parameter results in symmetric behaviors at the centerline of the channel for the velocity, temperature and concentration distributions. Tanveer *et al*. [20] studied the peristaltic motion of a Sisko fluid with homogeneous-heterogeneous reaction effects. The results revealed that the lower velocity, temperature and concentration profiles are obtained in case of the higher bending. Tanveer *et al*. [21] studied the peristaltic flow of Eyring-Powell nanofluids in a curved channel with compliant walls. They found that the Eyring-Powell parameters tend to decrease the velocity and temperature of the nanofluid while the concentration bears a dual response. Hayat *et el*. [22] discussed the peristalsis of MHD Jeffery nanofluids in a curved channel with a porous medium.

In a related context, there are several practical applications in atmospheric, engineering and physiological fields can be found for the dusty mixture such as conveying of powdered materials, purification of crude-oil, environmental pollutants, dust in gas cooling systems, petroleum industry. Rudinger [23] presented a valuable book that includes many other applications of the dusty mixture. Farbar and Morley [24] used a circular tube as a flow domain to examine the heat transfer convective flow of the gas-solid mixtures. The dusty model for the laminar flow was proposed by Saffman [25]. Various works [26-33] extended the dusty fluid topic with different physical circumstance. Recently, many researchers attempt to generalize these topics in case of the nanofluids. Siddiqa *et al*. [34] conducted an analysis of a two-phase natural-convection flow of dusty nanofluid along a vertical wavy surface. They found that presence of the dust particles have a notable influence on the temperature distribution as the isotherms get stronger for the dusty water. Begum *et al*. [35] studied the gyrotactic bioconvection of the dusty nanofluid along an isothermally heated vertical wall. They applied a numerical treatment for the mathematical model using the two-point implicit finite difference method. Gireesha *et al*. [36], Gireesha *et al*. [37] studied the Hall effect on a two-phase transient flow with stretching sheet using KVL model and irregular heat generation/consumption, respectively. The references [38, 39] handle interesting studies in these topics.

In all of the aforementioned works, the magnetic peristaltic motion of the dusty hybrid nanofluids in complex channels is ignored. Therefore, this paper aims to present comprehensive simulations for the MHD convective peristaltic flow of a hybrid nanofluid within a curved channel. Water is assumed as a base fluid while hybrid nanoparticles of Cu and Al are used as well as the one phase model is applied to simulate this situation. During the formulation of the problem the approximation of the low Reynolds number and the long wave length are taken into account. Also, one of the objectives of this study is to express the pressure distributions in the flow domain and examining effects of the dusty and geometry parameters on the hybrid nanofluid-flow and temperature distributions.

Discerption of the problem and mathematical formulation

The time-dependent 2-D peristaltic flows of dusty hybrid nanofluids within curved channels are considered. The physical model of the channel and the co-ordinates system are depicted in fig. 1. In order to formulate the governing systems of the problem, the following assumptions are considered:

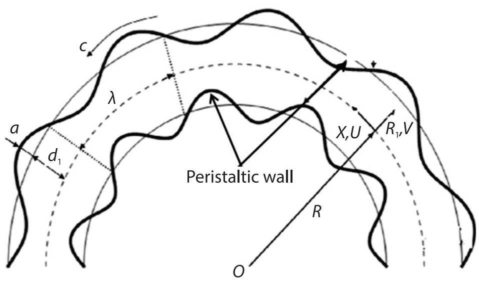

Figure 1. The physical model of the channel

- The X-axis is considered along the wall of the channel while the R-axis is considered normal to the channel surface.
- Width of the channel is $2d_1$ surrounded in a circle of a radius R and a center O.
- The mathematical formulation of the irregular boundaries of the channel is $\overline{\eta} = \pm [d_1 + a\sin(X - ct)(2\pi/\lambda)]$ where c, a, and λ are the speed, amplitude, and length of the wave.
- The components of the suspension are water as a based nanofluid and hybrid of Cu and Al_2O_3 nanoparticles.
- Table 1 shows the values of the thermophysical properties of the mixture components.
- A thermal equilibrium model is considered between the base fluid and the hybrid nanoparticles.
- The magnetic field, Joule heating, and viscous dissipation impacts are taken into account.
- The linear Boussinesq approximation is applied for the suspension density.
- Uniform sizes of the dusty particles are assumed and they distribute equally in the mixture.

Table 1. Values of the base fluid and nanoparticles thermophysical properties

Property	H_2O	Al_2O_3	Cu
ρ	997.1	3970	8933
c_p	4179	765	385
k	0.613	40	401
β	$21 \cdot 10^{-5}$	$0.85 \cdot 10^{-5}$	$1.67 \cdot 10^{-5}$
σ	0.05	$1 \cdot 10^{-10}$	$5.96 \cdot 10^{7}$

Under all the aforementioned assumptions, the governing equations of the problem are introduced as, see [14, 26, 27]:

– *Hybrid nanofluid phase*

$$\frac{\partial V}{\partial R}+\frac{R_1}{R+R_1}\frac{\partial U}{\partial X}+\frac{V}{R+R_1}=0 \tag{1}$$

$$\rho_{hnf}\frac{\partial V}{\partial t}+V\frac{\partial V}{\partial R}+\frac{UR_1}{R+R_1}\frac{\partial V}{\partial X}-\frac{U^2}{R+R_1}=$$

$$=-\frac{\partial P}{\partial R}+\frac{\mu_{hnf}}{R+R_1}\left[\frac{\partial}{\partial R}\left\{\left(R+R_1\right)\tau_{RR}\right\}+\frac{R_1}{R+R_1}\frac{\partial\tau_{XR}}{\partial X}-\frac{\tau_{XX}}{R+R_1}\right]+\frac{\rho_s}{\tau_m}\left(V_s-V\right) \tag{2}$$

$$\rho_{hnf}\left[\frac{\partial U}{\partial t}+V\frac{\partial U}{\partial R}+\frac{UR_1}{R+R_1}\frac{\partial U}{\partial X}+\frac{UV}{R+R_1}\right]=-\frac{R_1}{R+R_1}\frac{\partial P}{\partial X}+\frac{\mu_{hnf}}{\left(R+R_1\right)^2}\frac{\partial}{\partial R}\cdot$$

$$\cdot\left\{\left(R+R_1\right)^2\tau_{RX}\right\}+\left(\rho\beta\right)_{hnf}\mathrm{g}\left(T-T_0\right)+\frac{\mu_{hnf}R_1}{R+R_1}\frac{\partial\tau_{XX}}{\partial X}+\frac{\rho_s}{\tau_m}\left(U_s-U\right)-\frac{\sigma_{hnf}B_0^2}{R+R_1}U \tag{3}$$

$$\frac{\partial T}{\partial t}+V\frac{\partial T}{\partial R}+\frac{UR_1}{R+R_1}\frac{\partial T}{\partial X}=\frac{k_{hnf}}{\left(\rho c_p\right)_{hnf}}\nabla^2T+\frac{\mu_{hnf}}{\left(\rho c_p\right)_{hnf}}\cdot$$

$$\cdot\left[4\left(\frac{\partial V}{\partial R}\right)^2+\left(\frac{\partial U}{\partial R}+\frac{U}{R+R_1}+\frac{\partial V}{\partial X}\right)^2\right]+\frac{\rho_s c_s}{\tau_t\left(\rho c_p\right)_{hnf}}\left(T_s-T\right)+\frac{\rho_s}{\tau_m\left(\rho c_p\right)_{hnf}}\cdot$$

$$\cdot\left[\left(U_s-U\right)^2+\left(V_s-V\right)^2\right]+\frac{\sigma_{hnf}B_0^2}{\left(\rho c_p\right)_{hnf}\left(R+R_1\right)^2}U^2 \tag{4}$$

– *Dusty particles*

$$\frac{\partial V_s}{\partial R}+\frac{R_1}{R+R_1}\frac{\partial U_s}{\partial X}+\frac{V_s}{R+R_1}=0 \tag{5}$$

$$\rho_s\left[\frac{\partial V_s}{\partial t}+V_s\frac{\partial V_s}{\partial R}+\frac{U_sR_1}{R+R_1}\frac{\partial V_s}{\partial X}-\frac{{U_s}^2}{R+R_1}\right]=-\frac{\partial P_s}{\partial R}-\frac{\rho_s}{\tau_m}\left(V_s-V\right) \tag{6}$$

$$\rho_s\frac{\partial U_s}{\partial t}+V_s\frac{\partial U_s}{\partial R}+\frac{U_sR_1}{R+R_1}\frac{\partial U_s}{\partial X}+\frac{U_sV_s}{R+R_1}=-\frac{R_1}{R+R_1}\frac{\partial P_s}{\partial X}-\frac{\rho_s}{\tau_m}\left(U_s-U\right) \tag{7}$$

$$\rho_s c_s\left[\frac{\partial T}{\partial t}+V_s\frac{\partial T}{\partial R}+\frac{U_sR_1}{R+R_1}\frac{\partial T}{\partial X}\right]=-\frac{\rho_s c_s}{\tau_t}\left(T_s-T\right) \tag{8}$$

where

$$\nabla^2=\frac{\partial^2}{\partial R^2}+\frac{1}{R+R_1}\frac{\partial}{\partial R}+\left(\frac{R_1}{R+R_1}\right)^2\frac{\partial^2}{\partial X^2}$$

$$\tau_{XX}=\mu_{hnf}\left(\frac{2R_1}{R+R_1}\frac{\partial U}{\partial X}+\frac{2V}{R+R_1}\right)$$

$$\tau_{XR}=\mu_{hnf}\left(\frac{R_1}{R+R_1}\frac{\partial V}{\partial X}-\frac{U}{R+R_1}+\frac{\partial U}{\partial R}\right),\quad \tau_{RR}=2\mu_{hnf}\frac{\partial V}{\partial R}$$

where U, V, U_s, V_s are the velocity components of the fluid and dust phase, in the laboratory frame (R, X), P, P_s are the pressure, of the fluid and dust phase, σ_{hnf} – the electrical conductivity, ρ_f, ρ_s are the density of the fluid and dust phase, μ – the dynamic viscosity, ν – the kinematic viscosity, k – the thermal conductivity, c_p – the specific heat at constant pressure, C – the concentration, T – the temperature of the fluid, α – the coefficient of linear thermal expansion of the fluid, β – the coefficient of expansion with concentration, and g – the acceleration due to gravity. If (r, x) and (u, v), (u_s, v_s) are the co-ordinates and velocity components in the wave frame then:

$$\begin{gathered}\bar{x} = X - ct, \;\; \bar{r} = R, \;\; \bar{u} = U - c, \;\; \bar{v} = V, \;\; \bar{P}(x) = P(X,t) \\ \bar{u}_\mathrm{s} = \bar{U}_\mathrm{s} - c, \;\; \bar{v}_\mathrm{s} = V_\mathrm{s}, \;\; \bar{P}_\mathrm{s}(x) = P_\mathrm{s}(X,t)\end{gathered} \tag{9}$$

Also, the following non-dimensional quantities are introduced:

$$\begin{gathered}x = \frac{\bar{x}}{\lambda}, \;\; r = \frac{\bar{r}}{d_1}, \;\; u = \frac{\bar{u}}{c}, \;\; v = \frac{\bar{v}}{c\delta}, \;\; \delta = \frac{d_1}{\lambda}, \;\; P = \frac{\bar{P}d_1^2}{c\mu\lambda}, \;\; \eta = \frac{\bar{\eta}}{d_1}, \;\; \epsilon = \frac{a}{d_1} \\ k = \frac{R_1}{d_1}, \;\; \phi = \frac{C - C_0}{C_0}, \;\; \theta = \frac{T - T_0}{T_0}, \;\; u_\mathrm{s} = \frac{\bar{u}_\mathrm{s}}{c}, \;\; v_\mathrm{s} = \frac{\bar{v}_s}{c\delta}, \;\; P_\mathrm{s} = \frac{\bar{P}_\mathrm{s} d_1^2}{c\mu\lambda}\end{gathered} \tag{10}$$

where the subscript s refers to the dusty phase and 0 refers to the conditions at the channels walls. Moreover, definitions of the stream function for the nanofluid phase ψ and the dusty particles phase $\bar{\psi}$ are expressed:

$$u_\mathrm{s} = -\frac{\partial \bar{\psi}}{\partial r}, \;\; u = -\frac{\partial \psi}{\partial r}, \;\; v_\mathrm{s} = \frac{\delta k}{r + k}\frac{\partial \bar{\psi}}{\partial x}, \;\; v = \frac{\delta k}{r + k}\frac{\partial \psi}{\partial x} \tag{11}$$

When the pervious equations, eqs. (9) and (10), are inserted in the systems of eqs. (1)-(8) and taking into account estimations of the low Reynolds number and long of the wave length, the governing systems are given:

– *Hybrid nanofluid phase*

$$\frac{\partial P}{\partial r} = 0 \tag{12}$$

$$\begin{gathered}-\frac{k}{r + k}\frac{\partial P}{\partial x} + \frac{\mu_{hnf}}{\mu_f}\frac{\rho_\mathrm{f}}{\rho_{hnf}}\frac{1}{(r + k)^2}\frac{\partial}{\partial r}\left\{(r + k)^2\left[-\psi_{rr} - \frac{(1 - \psi_r)}{r + k}\right]\right\} + \\ + \frac{(\rho\beta)_{hnf}}{(\rho\beta)_\mathrm{f}}\mathrm{Gr}\,\theta + D_\mathrm{s}\alpha_d(\bar{\psi}_r - \psi_r) - \frac{\sigma_{hnf}}{\sigma_\mathrm{f}(r + k)}\mathrm{Ha}^2(1 - \psi_r) = 0\end{gathered} \tag{13}$$

$$\begin{gathered}\frac{1}{\mathrm{Pr}}\frac{(\rho c_p)_f}{(\rho c_p)_{hnf}}\frac{k_{hnf}}{k_\mathrm{f}}\left[\frac{\partial^2\theta}{\partial r^2} + \frac{1}{r + k}\frac{\partial\theta}{\partial r}\right] + \mathrm{Ec}\frac{(\rho c_p)_f}{(\rho c_p)_{hnf}}\frac{\mu_{hnf}}{\mu_\mathrm{f}}\left(-\psi_{rr} + \frac{\psi_r - 1}{r + k}\right)^2 + \frac{2}{3\mathrm{Pr}}\frac{(\rho c_p)_f}{(\rho c_p)_{hnf}}\cdot \\ \cdot D_\mathrm{s}\alpha_d(\theta_\mathrm{s} - \theta) + \frac{(\rho c_p)_f}{(\rho c_p)_{hnf}}D_\mathrm{s}\alpha_d\mathrm{Ec}(\bar{\psi}_r - \psi_r)^2 + \frac{\sigma_{hnf}}{\sigma_f}\frac{(\rho c_p)_f}{(\rho c_p)_{hnf}}\mathrm{Ec}\,\mathrm{Ha}^2\frac{1}{(r + k)^2}(1 - \psi_r)^2 = 0\end{gathered} \tag{14}$$

– *Dusty particles*

$$\frac{\partial P_\mathrm{s}}{\partial r} = 0 \tag{15}$$

$$0 = -\frac{k}{r + k}\frac{\partial P_\mathrm{s}}{\partial X} - \alpha_d(\bar{\psi}_r - \psi_r) \tag{16}$$

$$0=\left(\theta_{\mathrm{s}}-\theta\right) \tag{17}$$

where

$$\begin{gathered}\Pr=\frac{\nu_{\mathrm{f}}\left(\rho c_p\right)_f}{\kappa_f},\ \mathrm{Re}=\frac{\rho_{fcd_1}}{\mu_f},\ \mathrm{Ec}=\frac{\rho_f c^2}{\left(\rho c_p\right)_f T_0},\ \mathrm{Gr}=\frac{d_1^2 \mathrm{g}\left(\rho\beta\right)_f T_0}{\mu_f c} \\ \mathrm{Ha}^2=\frac{B_0^2 d_1^2\sigma_f}{\mu_f},\ \gamma=\frac{c_{\mathrm{s}}}{c_p},\ \alpha_d=\frac{d_1^2}{\tau_m \nu},\ \tau_t=\frac{3}{2}\tau_m\gamma\Pr,\ D_{\mathrm{s}}=\frac{\rho_{\mathrm{s}}}{\rho_f}\end{gathered} \tag{18}$$

where Pr is the Prandtl number, Re – the Reynolds number, Ec – the Eckert number, Gr – the Grashof number, Ha – the Hartman number, γ – the specific heat ratio of the mixture, D_s – the mass concentration of particle phase and α_d – the dust parameter. Also, eqs. (12), (13), (15), and (16) after eliminating the pressure terms are written:

$$\begin{gathered}\frac{\mu_{hnf}}{\mu_{\mathrm{f}}}\left[\left(r+k\right)\psi_{rrrr}+2\psi_{rrr}-\frac{\psi_{rr}}{r+k}+\frac{\psi_r}{\left(r+k\right)^2}\right]-\left(r+k\right)\cdot \\ \cdot\left\{\mathrm{Gr}\frac{\left(\rho\beta\right)_{hnf}}{\left(\rho\beta\right)_{bf}}\frac{\partial\theta}{\partial r}+D_{\mathrm{s}}\alpha_d\left(\frac{\partial\overline{\psi}_r}{\partial r}-\frac{\partial\psi_r}{\partial r}\right)+\frac{\sigma_{hnf}\,\mathrm{Ha}^2}{\sigma_f\left(r+k\right)^2}\left[\left(1-\psi_r\right)+\left(r+k\right)\psi_{rr}\right]\right\}- \\ -\left\{\mathrm{Gr}\frac{\left(\rho\beta\right)_{hnf}}{\left(\rho\beta\right)_{bf}}\theta+D_{\mathrm{s}}\alpha_d\left(\overline{\psi}_{r}-\psi_r\right)-\frac{\sigma_{hnf}}{\sigma_f\left(r+k\right)}\mathrm{Ha}^2\left(1-\psi_r\right)\right\}=\frac{\mu_{hnf}}{\mu_f}\frac{1}{\left(r+k\right)^2}\end{gathered} \tag{19}$$

$$\overline{\psi}_{rr}-\psi_{rr}+\frac{1}{r+k}\left(\overline{\psi}_r-\psi_r\right)=0 \tag{20}$$

$$\begin{gathered}\Delta P^*=k\int_0^1\left[\frac{\mu_{hnf}}{\mu_{\mathrm{f}}}\left(-\psi_{rr}-\frac{\left(1-\psi_r\right)}{r+k}\right)+\left(r+k\right)\cdot\right. \\ \left.\cdot\left(-\frac{\mu_{hnf}}{\mu_{\mathrm{f}}}\psi_{rrr}+\mathrm{Gr}\frac{\left(\rho\beta\right)_{hnf}}{\left(\rho\beta\right)_{bf}}\theta+D_{\mathrm{s}}\alpha_d\left(\overline{\psi}_r-\psi_r\right)-\frac{\sigma_{hnf}}{\sigma_{\mathrm{f}}\left(r+k\right)}\mathrm{Ha}^2\left(1-\psi_r\right)\right)\right]\mathrm{d}x\end{gathered} \tag{21}$$

– *The corresponding boundary conditions*

$$\psi=\mp\frac{F}{2},\ \frac{\partial\psi}{\partial r}=1,\ \theta=0,\ \phi=0,\ \overline{\overline{\psi}}=\mp\frac{F}{2},\ \frac{\partial\overline{\overline{\psi}}}{\partial r}=1,\ \theta_s=0\ \text{ at }\ r=\pm\left(1.+\epsilon\sin 2\pi X\right) \tag{22}$$

On the other hand, rate of the volume flows in the laboratory frame and in the wave frame are given, respectively:

$$Q=\int_{-\overline{\overline{\eta}}}^{\overline{\overline{\eta}}}U\left(R,X,t\right)\,\mathrm{d}R \tag{23}$$

$$q=\int_{-\overline{\overline{\eta}}}^{\overline{\overline{\eta}}}u\left(r,x\right)\mathrm{d}r \tag{24}$$

The dimensionless mean flows in the laboratory, Θ, and in the wave frame, F, are defined:

$$\Theta = \frac{\bar{Q}}{c d_1} \quad \text{and} \quad F = \frac{F}{c d_1} \tag{25}$$

where $\bar{Q}$ is the time averaged flow over a period $\bar{T}$ and it is given:

$$\bar{Q} = \frac{1}{\bar{T}} \int_0^{\bar{T}} Q \, \mathrm{d}t \tag{26}$$

From the previous equations, the relations are obtained:

$$\Theta = F + 2 \tag{27}$$

$$F = \int_{-\bar{\bar{\eta}}}^{\bar{\bar{\eta}}} \psi_r \, \mathrm{d}r \tag{28}$$

Additionally, the hybrid nanofluid properties are evaluated according to the correlations:

$$\rho_{hnf} = \phi_{\mathrm{Al_2O_3}} \rho_{\mathrm{Al_2O_3}} + \phi_{\mathrm{Cu}} \rho_{\mathrm{Cu}} + (1-\phi)\rho_{bf} \tag{29a}$$

$$(\rho c_p)_{hnf} = \phi_{\mathrm{Al_2O_3}} (\rho c_p)_{\mathrm{Al_2O_3}} + \phi_{\mathrm{Cu}} (\rho c_p)_{\mathrm{Cu}} + (1-\phi)(\rho c_p)_{bf} \tag{29b}$$

$$(\rho\beta)_{hnf} = \phi_{\mathrm{Al_2O_3}} (\rho\beta)_{\mathrm{Al_2O_3}} + \phi_{\mathrm{Cu}} (\rho\beta)_{\mathrm{Cu}} + (1-\phi)(\rho\beta)_{bf} \tag{29c}$$

$$\alpha_{hnf} = \frac{k_{hnf}}{(\rho c_p)_{hnf}} \tag{29d}$$

$$\frac{k_{hnf}}{k_{bf}} = \left[\frac{(\phi_{\mathrm{Al_2O_3}} k_{\mathrm{Al_2O_3}} + \phi_{\mathrm{Cu}} k_{\mathrm{Cu}})}{\phi} + 2k_{bf} + 2(\phi_{\mathrm{Al_2O_3}} k_{\mathrm{Al_2O_3}} + \phi_{\mathrm{Cu}} k_{\mathrm{Cu}}) - 2\phi k_{bf} \right] \cdot$$
$$\cdot \left[\frac{(\phi_{\mathrm{Al_2O_3}} k_{\mathrm{Al_2O_3}} + \phi_{\mathrm{Cu}} k_{\mathrm{Cu}})}{\phi} + 2k_{bf} - (\phi_{\mathrm{Al_2O_3}} k_{\mathrm{Al_2O_3}} + \phi_{\mathrm{Cu}} k_{\mathrm{Cu}}) + \phi k_{bf} \right]^{-1} \tag{29e}$$

$$\mu_{hnf} = \frac{\mu_{bf}}{\left[1 - (\phi_{\mathrm{Al_2O_3}} + \phi_{\mathrm{Cu}})\right]^{2.5}} \tag{29f}$$

$$\frac{\sigma_{hnf}}{\sigma_{\mathrm{f}}} = 1 + \frac{3\left[\dfrac{(\phi_{\mathrm{Al_2O_3}} \sigma_{\mathrm{Al_2O_3}} + \phi_{\mathrm{Cu}} \sigma_{\mathrm{Cu}})}{\sigma_f} - (\phi_{\mathrm{Al_2O_3}} + \phi_{\mathrm{Cu}}) \right]}{\left[\dfrac{(\phi_{\mathrm{Al_2O_3}} \sigma_{\mathrm{Al_2O_3}} + \phi_{\mathrm{Cu}} \sigma_{\mathrm{Cu}})}{\phi \sigma_f} + 2 \right] - \left[\dfrac{(\phi_{\mathrm{Al_2O_3}} \sigma_{\mathrm{Al_2O_3}} + \phi_{\mathrm{Cu}} \sigma_{\mathrm{Cu}})}{\sigma_f} - (\phi_{\mathrm{Al_2O_3}} + \phi_{\mathrm{Cu}}) \right]} \tag{29g}$$

Method of solution

To solve the governing equations (14), (15), (18), (20), and (21), it is needed to map the wavy boundaries into a rectangular computational domain. Therefore, the following new independent variables are introduced:

$$\xi = X, \quad \eta' = \frac{r}{1 + \epsilon \sin 2\pi X} \tag{30}$$

– *The partial derivatives for the dependent variables are obtained*

$$\begin{bmatrix} \dfrac{\partial \Phi}{\partial X} \\ \dfrac{\partial \Phi}{\partial r} \end{bmatrix} = \frac{1}{|J|} \begin{bmatrix} \beta_{11} & \beta_{12} \\ \beta_{21} & \beta_{22} \end{bmatrix} \begin{bmatrix} \dfrac{\partial \Phi}{\partial \xi} \\ \dfrac{\partial \Phi}{\partial \eta'} \end{bmatrix} \tag{31}$$

where

$$\beta_{11} = \frac{\partial r}{\partial \eta'}, \quad \beta_{12} = -\frac{\partial r}{\partial \xi}, \quad \beta_{21} = -\frac{\partial X}{\partial \eta'}, \quad \beta_{22} = \frac{\partial X}{\partial \xi} \text{ and } |J| = \beta_{11}\beta_{22} - \beta_{21}\beta_{12}$$

Using eqs. (30) and (31), the computational domain is transformed to $-1 \leq \eta' \leq 1$ which makes the applying of the numerical method is available. Here the Runge-Kutta method with shooting technique is used to solve the resulting system of the equations. The number of the grid points are taken to be equal 401 and the convergence criteria is 10^{-6}. In addition, a validation test consisting of comparisons with previously published results is performed and presented in fig. 2. It is found very good agreements are observed between the presented study (in special cases) and those obtained by Hina *et al.* [14].

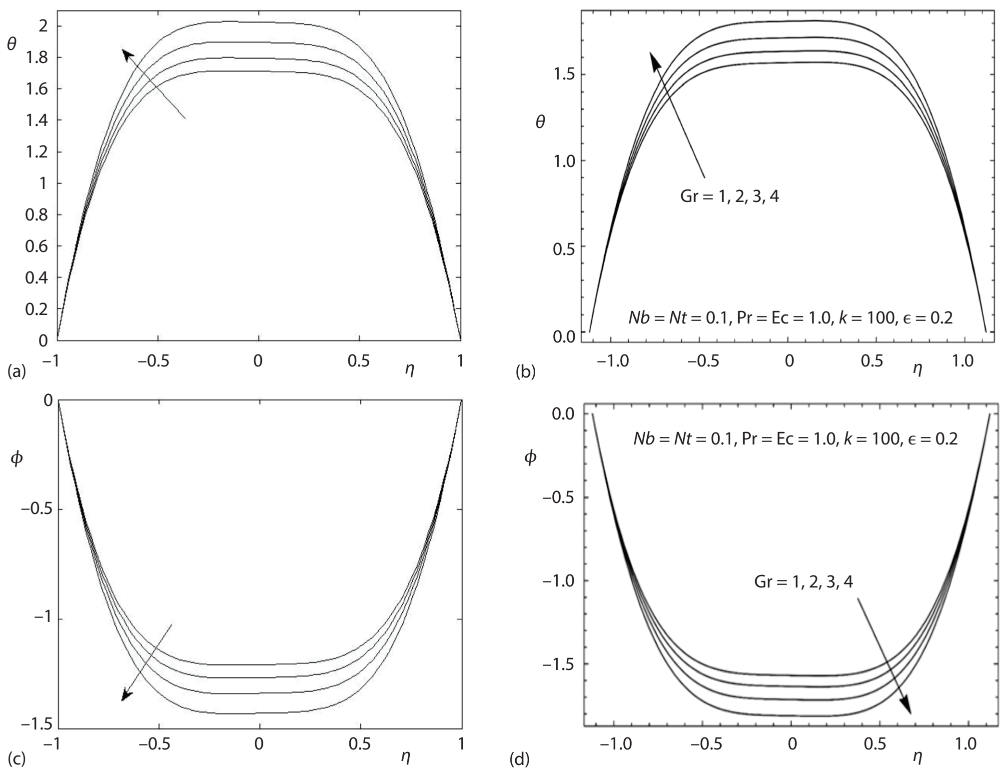

Figure 2. Validation tests at $\alpha_d = 0$ and $D_s = 0$; (a) present results and (b) [14]

Results and discussion

Discussion of the obtained results is notified in this section. A set of graphical results in terms of the velocity profiles for the dusty particles, temperature distributions and nanoparticle volume fraction are presented in figs. 3-16. During these computations, the governing parameters are considered in wide ranges *i.e.* range of the thermal buoyancy parameter $1 \le \mathrm{Gr} \le 4$, range of the Hartmann parameter is $0 \le \mathrm{Ha} \le 4$, range of amplitude ratio is $1 \le \epsilon \le 5$, range the Eckert number is $0.1 \le \mathrm{Ec} \le 0.5$ and range of the Cu nanoparticles is $0 \le \phi_{\mathrm{Cu}} \le 0.05$. Here it should be mentioned that from eq. (17), the profiles of the temperature of the dusty particles are the same of nanofluid temperature. Also, values of the mass concentration of the dusty particles, D_s, and the dusty parameters, α_d, are assumed 0.1 and 10, respectively.

Figures 3-5 show the profiles of the fluid velocity, dusty velocity and fluid temperature for various values of Hartmann number at $\mathrm{Gr} = 1$, $\epsilon = 0.2$, $\mathrm{Ec} = 1$, $\mathrm{Pr} = 6.82$, $k = 5$, $\alpha_d = 10$, $D_s = 0.1$, $\phi_{\mathrm{Cu}} = 0.01$.The results revealed that the growing in the magnetic parameter causes a diminishing in the convective process and hence both of the fluid and dusty velocities are reduced. Physically, these behaviors are due to the Lorentz force resulting from the magnetic field that works against to the hybrid nanofluid-flow. On the contrary, the temperature distributions are enhanced as Hartmann number is increased due to the increase in the thermal boundary-layer as the magnetic force is enhanced.

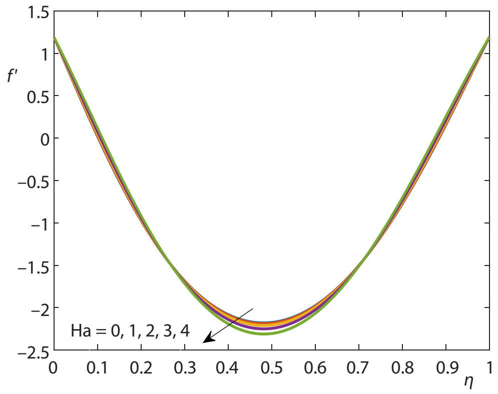

Figure 3. Fluid velocity for different values of Ha at Gr = 1, ϵ = 0.2, Ec = 1, Pr = 6.82, k = 5, α_d = 10, D_s = 0.1, ϕ_{Cu} = 0.01

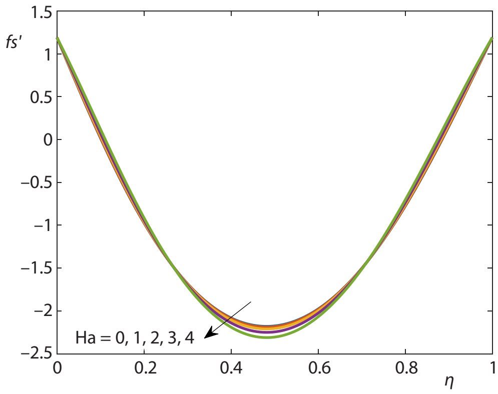

Figure 4. Dusty velocity for different values of Ha at Gr = 1, ϵ = 0.2, Ec = 1, Pr = 6.82, k = 5, α_d = 10, D_s = 0.1, ϕ_{Cu} = 0.01

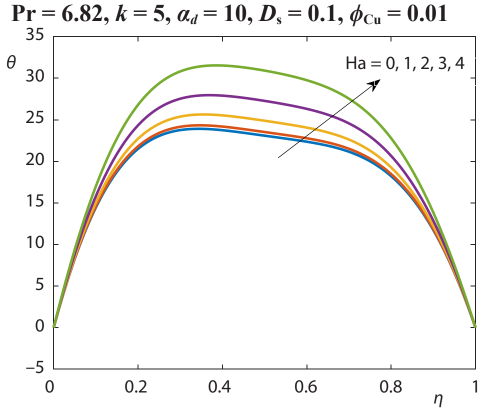

Figure 5. Profiles of the fluid temperature for different values of Ha at Gr = 1, ϵ = 0.2, Ec = 1, Pr = 6.82, k = 5, α_d = 10, D_s = 0.1, ϕ_{Cu} = 0.01

Figures 6-8 display the hybrid nanofluid velocity, dusty velocity and mixture temperature for various values of Grashof number at $\phi_{\mathrm{Cu}} = 0.01$, $\epsilon = 0.2$, Ec = 1, Pr = 6.82, $k = 5$, $\alpha_d = 10$, $D_s = 0.1$, and Ha = 1. It is noted that in the rage $0.25 \leq \eta \leq 0.75$, the alteration of Gr causes that the hybrid nanofluid and dusty velocities tend to decrease while the inverse behaviors are noted for the other values of η. Additionally, the hybrid nanofluid temperature is increasing as Gr is growing, for all values of η.

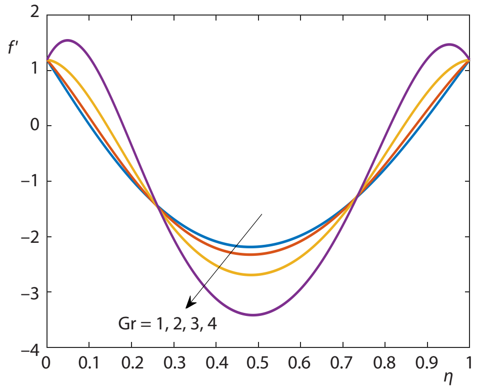

Figure 6. Fluid velocity for different values of Gr at $\phi_{\mathrm{Cu}} = 0.01$, $\epsilon = 0.2$, Ec = 1, Pr = 6.82, $k = 5$, $\alpha_d = 10$, $D_s = 0.1$, and Ha = 1

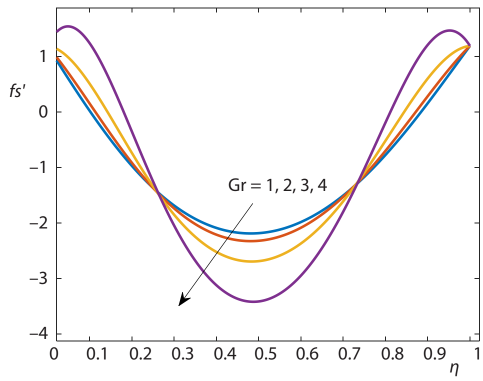

Figure 7. Dusty velocity for different values of Gr at $\phi_{\mathrm{Cu}} = 0.01$, $\epsilon = 0.2$, Ec = 1, Pr = 6.82, $k = 5$, $\alpha_d = 10$, $D_s = 0.1$, and Ha = 1

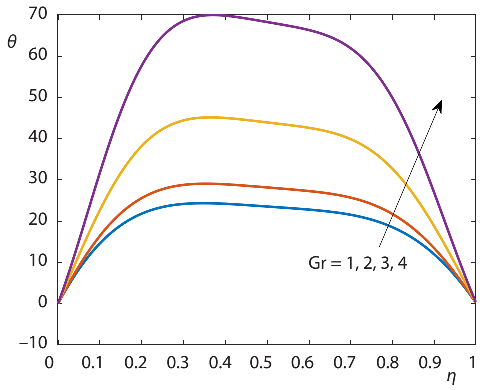

Figure 8. Profiles of the fluid temperature for different values of Gr at $\phi_{\mathrm{Cu}} = 0.01$, $\epsilon = 0.2$, Ec = 1, Pr = 6.82, $k = 5$, $\alpha_d = 10$, $D_s = 0.1$, and Ha = 1

Profiles of the hybrid nanofluid velocity, dusty velocity and the suspension temperature for various values of amplitude ratio at $\phi_{\mathrm{Cu}} = 0.01$, Gr = 1, Ec = 1, Pr = 6.82, $k = 5$, $\alpha_d = 10$, $D_s = 0.1$, and Ha = 1 are displayed in figs. 9-11. Like impacts of Grashof number on the hybrid nanofluid and dusty velocities, the variations of ϵ reduces the velocity components in the range $0.25 \leq \eta \leq 0.75$ while these componenets are enhanced in the remaining values of η. Furthermore, a clear enhancement in the temperature distributions is given as the amplitude ratio η is growing. The increasing behaviors of the temperature are noted for all values of η with higher variations of the temperature when ϵ is altered from 0.8 to 1 comparing to the other values of ϵ.

In figs. 12-14, impacts of the curvature parameter, k, on the velocities of the hybrid nanofluids and dusty phases together with the temperature distributions at $\phi_{\mathrm{Cu}} = 0.01$, Gr = 1, Ec = 1, Pr = 6.82, $\alpha_d = 10$, $D_s = 0.1$, Ha = 1, and $\epsilon = 0.2$ are displayed in figures are illustrated. The findings disclosed that there are two opposite behaviors are observed as k is increased.

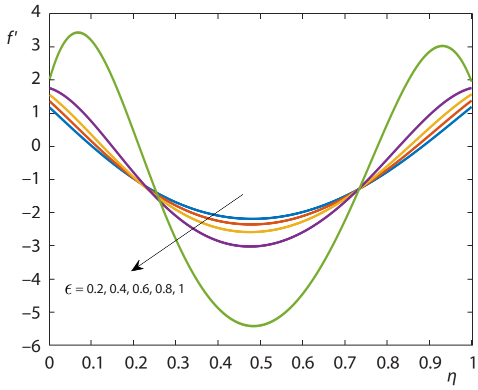

Figure 9. Fluid velocity for different values of ϵ at $\phi_{Cu} = 0.01$, Gr = 1, Ec = 1, Pr = 6.82, $k = 5$, $\alpha_d = 10$, $D_s = 0.1$, and Ha = 1

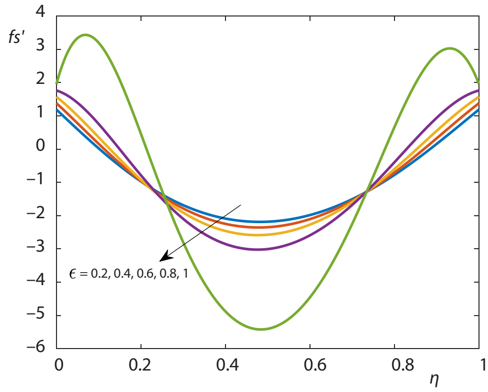

Figure 10. Dusty fluid velocity for different values of ϵ at $\phi_{Cu} = 0.01$, Gr = 1, Ec = 1, Pr = 6.82, $k = 5$, $\alpha_d = 10$, $D_s = 0.1$, and Ha = 1

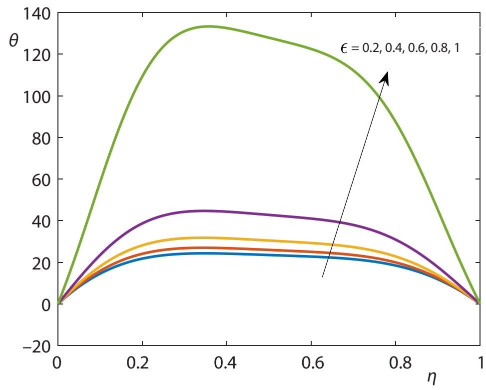

Figure 11. Profiles of the fluid temperature for different values of ϵ at $\phi_{Cu} = 0.01$, Gr = 1, Ec = 1, Pr = 6.82, $k = 5$, $\alpha_d = 10$, $D_s = 0.1$, and Ha = 1

Those are enhancements of the velocities as k is growing in the lower part of the channel and a weakness in the flows as k increases in the upper parts of the channel. However, the temperature distributions are diminishing as k is altered in the whole domain. All these behaviors show that the curvature parameter is a good factor in controlling the flow and thermal fields.

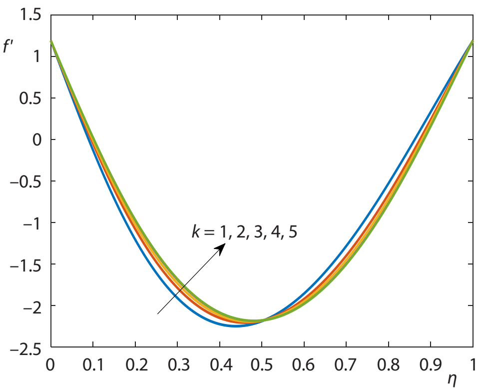

Figure 12. Fluid velocity for different values of k at $\phi_{Cu} = 0.01$, Gr = 1, Ec = 1, Pr = 6.82, $\alpha_d = 10$, $D_s = 0.1$, Ha = 1, and $\epsilon = 0.2$

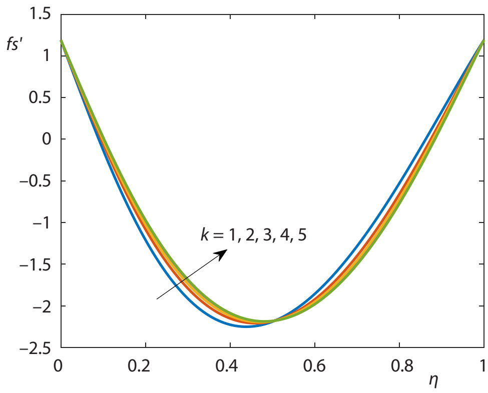

Figure 13. Dusty velocity for different values of k at $\phi_{Cu} = 0.01$, Gr = 1, Ec = 1, Pr = 6.82, $\alpha_d = 10$, $D_s = 0.1$, Ha = 1, and $\epsilon = 0.2$

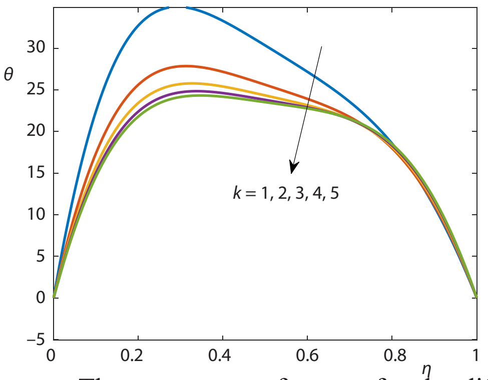

Figure 14. Profiles of the fluid temperature for different values of k at $\phi_{Cu} = 0.01$, Gr = 1, Ec = 1, Pr = 6.82, $\alpha_d = 10$, $D_s = 0.1$, Ha = 1, and $\epsilon = 0.2$

The temperature features for the different values of the Eckert number and the Cu nanoparticles volume fraction ϕ_{Cu} at Gr = 1, $k = 5$, Pr = 6.82, $\alpha_d = 10$, $D_s = 0.1$, Ha = 1, and $\epsilon = 0.2$ are displayed in figs. 15 and 16. The results revealed that the temperature distributions are augmented as Eckert number is increased. Physically, the growing in Eckert number means the increase in the viscous dissipation process which heated up the mixture and hence the temperature distributions are enhanced. On the contrary, the growing in ϕ_{Cu} makes the mixture more viscous and thus the convective process is reduced and as a result the temperature distributions are diminishing as ϕ_{Cu} is increasing.

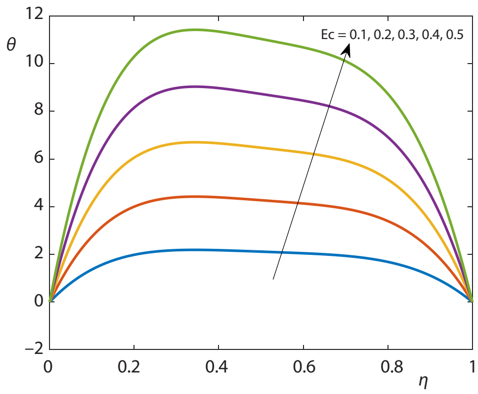

Figure 15. Profiles of the fluid temperature for different values of Ec at $\phi_{Cu} = 1$, Gr = 1, $k = 5$, Pr = 6.82, $\alpha_d = 10$, $D_s = 0.1$, Ha = 1, and $\epsilon = 0.2$

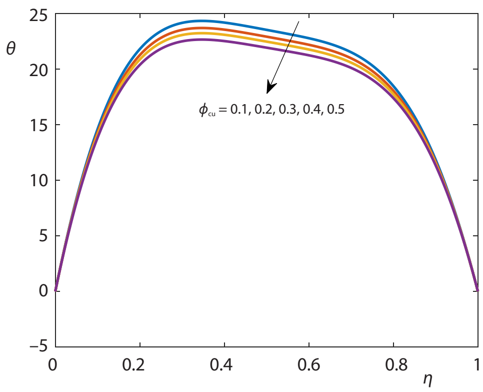

Figure 16. Profiles of the fluid temperature for different values of ϕ_{Cu} at Gr = 1, $\epsilon = 0.2$, Ec = 1, $k = 5$, Pr = 6.82, $\alpha_d = 10$, $D_s = 0.1$, Ha = 1

Conclusions

The current study carried out numerical simulations for the magnetic convective peristaltic flow of a dusty hybrid nanofluid in curved channels. The low Reynolds number and the long wave length approach are assumed. Two systems of the equations are presented for the hybrid nanofluid and the dusty particles phases. A mathematical form for the pressure distributions is introduced and validation tests with previously published results are performed. The main outcomes of this study can be summarized as follows.

- The temperature lineaments are supported as either the Hartmann number or the Grashof number are growing.

- An increase in the Eckert number enhances the viscous dissipation process and hence the temperature distributions tend to increase.
- A weakness hybrid nanofluid and dusty flows are given as the magnetic force is enhanced.
- Values of the dusty temperature are equal values of the nanofluid temperature regardless variations of the governing parameter.
- Velocity of the dusty particles is reduced as the Grashof number and the amplitude ratio increase (particularly at the mid-section of the channel).
- The current study can be extended in the future to include the radiation impacts, variable magnetic field and non-linear Boussinesq approximation.

Acknowledgment

The authors extend their appreciation the Deanship of Scientific Research at King Khalid University for funding this work through research groups program under Grant Number (R.G.P2/27/42).

Nomenclature

a – dimensional wave amplitude
c – wave speed
c_p – specific heat at constant pressure
C – concentration
d_1 – thickness of the channel
D_s – mass concentration of the dust particle
Ec – Eckert number
g – gravity acceleration
Gr – Grashov number
Ha – Hartmann number
k – curvature parameter
P – pressure
Pr – Prandtl number
R_1 – radius parameter
Re – Reynolds number
T – temperature, [K]
t – time
(U, V) – velocity components in the R and X direction
(R, X) – dimensional Cartesian co-ordinates
(r, x) – dimensionless Cartesian co-ordinates

Greek symbols

α – coefficient of linear thermal expansion
α_d – dust parameter depending on the relaxation time of the particles and the buoyancy force
β – coefficient of thermal expansion
δ – wave number
ϵ – amplitude ratio
θ – dimensionless temperature
κ – thermal conductivity
λ – wave length
μ – dynamic viscosity
ν – kinematic viscosity
ρ – density
σ – superficial tension, [Nm^{-1}]
τ_m – momentum relaxation time
τ_t – thermal relaxation time
ϕ – nanoparticle volume fraction
ψ – stream function

Subscripts

f – fluid
P – nanoparticle
s – dusty

References

[1] Latham, T., Fluid Motions in a Peristaltic Pump, M. S. thesis, MIT, Cambridge, Mass., USA, 1966
[2] Misra, J., Pandey, S., Peristaltic Transport of Physiological Fluids, in: *Biomathematics: Modelling and Simulation*, (Ed. J. C. Misra), World Scientific, London, USA, Singapore, 2006, pp. 167-193 (Chapter 7)
[3] Sato, H., *et al*., The 2-D Peristaltic Flow in Curved Channels, *Trans. Jpn. Soc. Mech. Eng*., *B 66* (2000), 643, pp. 679-685
[4] Ali, N., *et al*., Long Wavelength Flow Analysis on Curved Channel, *Z. Naturforsch*, *A 65* (2010), 3, pp. 191-196
[5] Ali, N., *et al*., Heat Transfer Analysis of Peristaltic Flow in a Curved Channel, *Int. J. Heat Mass Trans*., *53* (2010), 15-16, pp. 3319-3325
[6] Ali, N., *et al*., Non-Newtonian Fluid-Flow Induced by Peristaltic Waves in a Curved Channel, *Europ. J. Mech- B/Fluids*, *29* (2010), 5, pp. 387-394

[7] Hayat, T., *et al*., Peristaltic Transport of Viscous Fluid in a Curved Channel with Compliant Walls, *Int. J. Heat Mass Transf., 54* (2011), 7, pp. 1615-1621

[8] Hayat, T., *et al*., Effect of Wall Properties on the Peristaltic Flow of a Third Grade Fluid in a Curved Channel with Heat and Mass Transfer, *Int. J. Heat Mass Transf*., *54* (2011), 23-24, pp. 5126-5136

[9] Hina, S., *et al*., Peristaltic Transport of Johnson-Segalman Fluid in a Curved Channel with Wall Compliant Properties, *Non-linear Anal: Model Control*, *17* (2012), 3, pp. 297-311

[10] Hina, S., *et al*., Heat and Mass Transfer Effects on the Peristaltic Flow of Johnson-Segalman Fluid in a Curved Channel with Compliant Walls, *Int. J. Heat Mass Transf*., *55* (2012), 13-14, pp. 3511-3521

[11] Hina, S., *et al*., Peristaltic Flow of Pseudoplastic Fluid in a Curved Channel with Wall Properties, *Journal Appl. Mech. Trans. ASME*, *80* (2013), 2, 024501

[12] Choi, S., Enhancing Thermal Conductivity of Fluids with Nanoparticles, in: *Developments and Applications of Non-newtonian Flows, American Society of Mechanical Engineers*, (Eds. D. A. Singer, H. P. Wamg), New York, USA, 1995, pp. 99-105

[13] Buongiorno, J., Convective Transport in Nanofluids, *ASME J. Heat Transf.*, *128* (2006), 3, pp. 240-250

[14] Hina, S., *et al*., Peristaltic Motion of Nanofluid in a Curved Channel, *Journal Heat Transfer – Trans ASME*, *136* (2014), 052001

[15] Ayub, S., *et al*., Thermal Radiation Impact in Mixed Convective Peristaltic Flow of Third Grade Nanofluid, *Results in Physics*, *7* (2017), Sept., pp. 3687-3695

[16] Narla, V., *et al*., Peristaltic Transport of Jeffrey Nanofluid in Curved Channels, *Procedia Engineering*, *127* (2015), pp. 869-876

[17] Noreen, S., *et al*., The MHD Pressure Driven Flow of Nanofluid Incurved Channel, *Journal of Magnetism and Magnetic Materials*, *393* (2015), May, pp. 490-497

[18] Hayat, T., *et al*., Mixed Convection Peristaltic Motion of Copper-Water Nanomaterial with Velocity Slip Effects in a Curved Channel, *Computer Methods and Programs in Biomedicine*, *142* (2017), Apr., pp. 117-128

[19] Hayat, T., *et al*., Numerical Study for MHD Peristaltic Transport of Sisko Nanofluid in a Curved Channel, *International Journal of Heat and Mass Transfer*, *109* (2017), Feb., pp. 1281-1288

[20] Tanveer, A., *et al*., Mixed Convective Peristaltic Flow of Sisko Fluid in Curved Channel with Homogeneous-Heterogeneous Reaction Effects, *Journal of Molecular Liquids*, *233* (2017), Mar., pp. 131-138

[21] Tanveer, A., *et al*., Mixed Convection Peristaltic Flow of Eyring-Powell Nanofluid in a Curved Channel with Compliant Walls, *Computers in Biology and Medicine*, *82* (2017), Mar., pp. 71-79

[22] Hayata, T., Numerical Analysis of Partial Slip on Peristalsis of MHD Jeffery Nanofluid in Curved Channel with Porous Space, *Journal of Molecular Liquids*, *224* (2016), Part A, pp. 944-953

[23] Rudinger, G., *Fundamentals of Gas-Particle Flow*, Elsevier Scientific Publishing Co., Amsterdam, The Netherlands, 1980

[24] Farbar, L., Morley, M., Heat Transfer to Flowing Gas-Solid Mixtures in a Circular Tube, *Ind. Eng. Chem., 49* (1957), 7, pp. 1143-1150

[25] Saffman, P., On the Stability of Laminar Flow of a Dusty Gas, *Journal Fluid Mech*., *13* (1962), 1, pp. 120-128

[26] Turkyilmazoglu, M., Magnetohydrodynamic Two-Phase Dusty Fluid-Flow and Heat Model over Deforming Isothermal Surfaces, *Phys. Fluids*, *29* (2017), 1, 013302

[27] Jalil, M., *et al*., An Exact Solution of MHD Boundary-Layer Flow of Dusty Fluid over a Stretching Surface, *Math. Probl. Eng*., *2017* (2017), ID2307469

[28] Gireesha, B., *et al.*, Study of Unsteady Dusty Fluid-Flow through Rectangular Channel in Frenet Frame Field System, *Int. J. Pure Appl. Math*., *34* (2007), 4, pp. 525-534

[29] Gireesha, B., *et al*., Pulsatile Flow of an Unsteady Dusty Fluid through Rectangular Channel, *Commun. Non-Linear Sci. Numer. Simulat*., *14* (2009), 5, pp. 2103-2110

[30] Manjunatha, P., *et al*., Thermal Analysis of Conducting Dusty Fluid-Flow in a Porous Medium over a Stretching Cylinder in the Presence of Non-Uniform Source/Sink, *Int. J. Mech. Mater. Eng*., *9*, (2014), Sept., 14

[31] Prasannakumar, B.. *et al*., Melting Phenomenon in MHD Stagnation Point Flow of Dusty Fluid over a Stretching Sheet in the Presence of Thermal Radiation and Non-Uniform Heat Source/Sink, *Int. J. Comput. Methods Eng. Sci Mech*., *16* (2015), 5, pp. 265-274

[32] Bagewadi, C., *et al.*, Boundary-Layer Flow of Dusty Fluid over a Radiating Stretching Surface Embedded in a Thermally Stratified Porous Medium in the Presence of Uniform Heat Source, *Non-Linear Eng*., *6* (2017), 1, pp. 31-41

[33] Muthuraj, R., *et al*., Influences of Chemical Reaction and Wall Properties on MHD Peristaltic Transport of a Dusty Fluid with Heat and Mass transfer, *Alexandria Engineering Journa*, *55* (2016), 1, pp. 597-611
[34] Siddiqa, S., *et al*., Two-Phase Natural-Convection Dusty Nanofluid-Flow, *International Journal of Heat and Mass Transfer*, *118* (2018), Mar., pp. 66-74
[35] Begum, N., *et al*., Numerical Solutions for Gyrotactic Bioconvection of Dusty Nanofluid Along a Vertical Isothermal Surface, *International Journal of Heat and Mass Transfer*, *113* (2017), Oct., pp. 229-236
[36] Gireesha, B., *et al*., Hall Effects on Dusty Nanofluid Two-Phase Transient Flow Past a Stretching Sheet Using KVL Model, *Journal of Molecular Liquids*, *256* (2018), Apr., pp. 139-147
[37] Gireesha, B., *et al*., Hall Effect on Two-Phase Radiated Flow of Magneto-Dusty-Nanoliquid with Irregular Heat Generation/Consumption, *Results in Physics*, *7* (2017), Sept., pp. 4340-4348
[38] Ahmed, S. E., *et al*., Unsteady Mixed Nanobioconvection Flow in a Horizontal Channel with Its Upper Plate Expanding or Contracting: A Revised Model, *Thermal Science*, *23* (2019), 5B, pp. 3283-3292
[39] Rashed, Z. Z., *et al*., Heat Transfer Enhancement in the Complex Geometries Filled with Porous Media, *Thermal Science*, *25* (2021), 1A, pp. 39-57

Paper submitted: October 14, 2019
Paper revised: February 15, 2021
Paper accepted: March 8, 2021

© 2021 Society of Thermal Engineers of Serbia
Published by the Vinča Institute of Nuclear Sciences, Belgrade, Serbia.
This is an open access article distributed under the CC BY-NC-ND 4.0 terms and conditions